Resolution and Mass Range Performance in Distance-of-Flight Mass Spectrometry with a Multichannel Focal-Plane Camera Detector

ARTICLE *in* ANALYTICAL CHEMISTRY · NOVEMBER 2011

Impact Factor: 5.64 · DOI: 10.1021/ac201876y · Source: PubMed

analytical chemistry

ARTICLE

pubs.acs.org/ac

Resolution and Mass Range Performance in Distance-of-Flight Mass Spectrometry with a Multichannel Focal-Plane Camera Detector

Alexander W. G. Graham,[†] Steven J. Ray,[†] Christie G. Enke,[†,‡] Jeremy A. Felton,[†] Anthony J. Carado,[§] Charles J. Barinaga,[§] David W. Koppenaal,[§] and Gary M. Hieftje*[,†]

[†]Department of Chemistry, Indiana University, Bloomington Indiana 47405, United States

[‡]Department of Chemistry, University of New Mexico, Albuquerque New Mexico 87131, United States

[§]Pacific Northwest National Laboratory, Richland Washington 99352, United States

ABSTRACT: Distance-of-flight mass spectrometry (DOFMS) is a velocity-based mass-separation technique in which ions are separated in space along the plane of a spatially selective detector. In the present work, a solid-state charge-detection array, the focal-plane camera (FPC), was incorporated into the DOFMS platform. Use of the FPC with our DOFMS instrument resulted in improvements in analytical performance, usability, and versatility over a previous generation instrument that employed a microchannel-plate/phosphor DOF detector. Notably, FPC detection provided resolution improvements of at least a factor of 2, with typical DOF linewidths of 300 μm ($R_{(fwhm)}$ = 1000). The merits of solid-state detection for DOFMS are evaluated, and methods to extend the DOFMS mass range are considered.

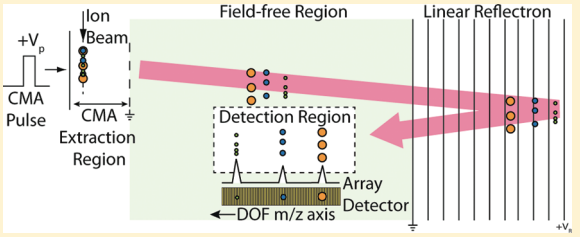

Velocity-based mass separations, such as distance-of-flight mass spectrometry (DOFMS) and time-of-flight mass spectrometry (TOFMS), offer a number of benefits over other mass spectrometry (MS) techniques, including a theoretically unlimited mass range, high spectral generation rates, simultaneous ion-packet analysis, and simple instrument design.[1] Put simply, TOFMS discriminates between ions of different mass-to-charge ratios (m/z) by accelerating ions to mass-dependent velocities and measuring ion flight times at a fixed distance. An alternative approach to velocity-based MS is to hold flight time constant and measure the flight distance; this is the basis of distance-of-flight mass spectrometry (DOFMS). While TOFMS provides temporal mass separation, DOFMS provides spatial mass separation.

Several advantages arise from separating ions in space rather than time. First, DOFMS eliminates the need for the fast ion detectors and time-discrimination electronics requisite to TOFMS. Second, DOFMS provides a platform for the incorporation of high dynamic-range, charge-detection arrays into velocity-based mass spectrometers. Third, spatial m/z separation offers the potential for simultaneous isolation and collection of ions of interest.

Thus far, two studies of DOFMS have been reported: the first outlines the theoretical framework behind DOFMS,[2] while the second provides initial results from the first DOFMS instrument.[3] These initial studies provide theoretical and experimental verification of the DOFMS method and also report in detail the operation of the instrument. The current paper extends DOFMS through the incorporation of a solid-state array detector.

BACKGROUND AND MOTIVATIONS

DOFMS Theory. To begin, we provide a brief overview of the fundamental principles of DOFMS that have guided the development and operation of our DOF mass spectrometer. A schematic diagram of our DOFMS instrument is provided in Figure 1. In DOFMS, ions are accelerated to a constant momentum, allowed to drift through a field-free region, turned around in a linear-field ion mirror, and while traversing a second field-free region are pushed upward (normal to the drift plane) at a given detection time onto the surface of a spatially selective detector. This detector measures the combined field-free flight distance (L) traveled by m/z-separated ion packets during a constant time interval (t).

For simplicity, let us first consider the relationship between m/z and distance of flight (DOF), which is equivalent to L, in the absence of an ion mirror. To start, we determine the m/z-dependent velocity produced by constant-momentum acceleration (CMA). In particular, CMA is achieved by application of a time-dependent linear acceleration field that is brief enough so all ions of interest are still within the extraction region at the cessation of the pulse.[4] CMA is then easily derived from fundamental principles: The force (f) experienced by an ion in the extraction region is given in eq 1:

$$f = qE_p = ma = m\frac{dv}{dt} \quad (1)$$

where q is the fundamental charge, E_p is the electric-field strength in the acceleration region, m is the ion mass, and dv/dt is the change in ion velocity with time (acceleration). In CMA, all ions experience the same force for the same time interval, so eq 1 can

Received: July 21, 2011
Accepted: October 5, 2011
Published: October 05, 2011

   dx.doi.org/10.1021/ac201876y | *Anal. Chem.* 2011, 83, 8552–8559

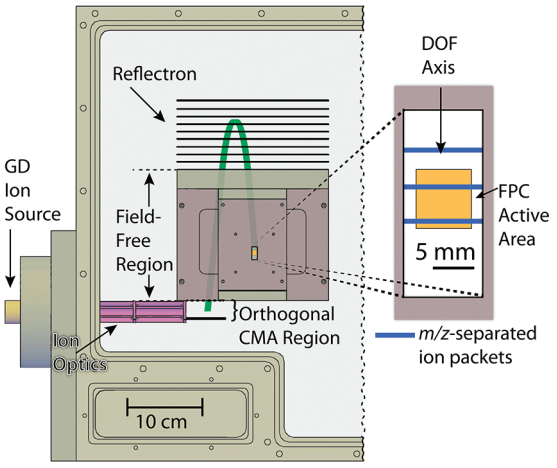

Figure 1. Mechanical drawing of the DOFMS instrument with ion flight path shown in green and a portion of the mass-analysis chamber cut out for clarity. As drawn, the *x*-axis is the initial ion-beam axis and mass separation occurs along the *y*-axis. The total field-free region is 282 mm from the exit of the constant-momentum acceleration (CMA) region to the DOF detector. In this paper, we report results collected when the focal-plane camera (FPC) is positioned above the distance-of-flight (DOF) extraction region, running coaxial to the mass-separation axis; the area of the 6.4-mm FPC is shown in yellow. The inset is a zoomed-in view of the DOF detection region with schematic depictions of mass-separated ion packets as blue bars. This inset illustrates the size of the FPC compared to typical DOFMS-separated ion packets.

be solved for dt and integrated to show that all m/z are given the same momentum mv:

$$mv = qE_p\tau \tag{2}$$

where v is the ion's final velocity and τ is the pulse length of the CMA field. From eq 2 we can find the field-free distance L ions traverse after the end of the CMA pulse during a given ion flight time t, which shows that DOF is inversely proportional to m/z:

$$\frac{m}{z} = \left(\frac{1}{L}\right)qE_p\tau t \tag{3}$$

Equations 2 and 3 assume that all ions start with zero initial velocity along the mass-separation axis. However, with any gaseous ion source there is a spread of initial ion velocities. With CMA, these initial velocities are superimposed on velocities attained from the CMA pulse and lead to variations in flight distance and a corresponding spread in peak widths and degradation of resolving power. Thus, in DOFMS, we employ a single-stage ion mirror to correct for this initial velocity spread. Specifically, the ion mirror serves as an energy-focusing device: ions with an initial velocity component toward the mass-separation axis penetrate deeper into, and spend more time in, the mirror than ions with no initial velocity or with a velocity opposing CMA extraction. When ions emerge from the mirror, there exists a point in time when ions that were initially forward-moving, stationary, or rearward-moving within the CMA source all come to a spatial focus. This time is known as the energy-focus time (t_{ef})[2] and is defined by instrumental parameters:

$$t_{ef} = \frac{4E_p\tau}{E_M} \tag{4}$$

where E_M is the electric-field strength in the ion mirror. The energy-focus time is valid for all m/z because the time spent in the mirror is a function of only ion-energy spread and not m/z. Additionally, because the CMA extraction field is turned off before any ions leave the source, initially rearward-moving ions do not gain the same energy as their forward-moving counterparts and thus the turn-around time error inherent to TOFMS[5] does not exist in constant-momentum DOFMS. Because t_{ef} includes the time ions spend in the mirror, the relationship between m/z and L is redefined for detection at t_{ef}:

$$\frac{m}{z} = \left(\frac{1}{L}\right)\frac{(2q(E_p\tau)^2)}{E_M} \tag{5}$$

Equation 5 illustrates several important points about DOFMS. First, flight distance provides an unequivocal measure of m/z if a position-sensitive ion detector simultaneously records ions of many m/z values across its surface. Second, since any real DOF detector must be of finite length and is likely to sit at a fixed location, various m/z-windows can be focused onto its surface by simple manipulation of electrostatic potentials: changing E_M, E_p, or τ will bring different mass ranges into focus at a stationary DOF detector. In this manner, a full mass spectrum can be acquired by sequentially collecting such m/z windows; alternatively, desired sections of the spectrum can be rapidly accessed by hopping between windows. Finally, the inverse relationship between m/z and flight length means that the measurement of mass resolving power (R) can be accomplished by taking the derivative of eq 5, which yields

$$R = \frac{m}{\Delta m} = \frac{L}{\Delta L} \tag{6}$$

DOFMS Detection Requirements. Though establishment of the energy-focus time provides a theoretical basis for performing DOFMS analysis, implementation of DOFMS also requires a suitable spatially selective detector to record the position of ion strikes along the mass-separation axis. Properties of the DOF detector directly affect mass-spectral resolution, accessible mass range, limits of detection, dynamic range, and simplicity and speed of spectral acquisition. Accordingly, important characteristics for DOFMS detectors include spatial resolution, active detection area, sensitivity, linear dynamic range, simultaneous detection capability, and readout time.

The most fundamental requirement for DOFMS detection is spatial selectivity. Several potentially appropriate ion detectors have been developed for use with sector-field mass spectrometers or imaging mass spectrometers.[6,7] Examples include photographic plates,[8] electro-optic imaging detectors (EOIDs),[9,10] resistive-anode detectors,[11] delay-line detectors,[12] and discrete-anode array detectors.[13] Unfortunately, each of these detection approaches has drawbacks that limit its usefulness for DOFMS detection. For instance, resistive anode or delay-line detectors often provide excellent spatial resolution but do so through the use of algorithms that necessitate a single ion strike per acquisition period; for DOFMS, ions of multiple m/z must be detected simultaneously across the length of the detector. In contrast, EOIDs provide simultaneous, two-dimensional ion detection with acceptable resolution. Yet, EOIDs are subject to peak broadening and lateral signal variation across the microchannel-plate (MCP)/phosphor assembly. As a solution, we propose that solid-state array detector technology best meets the needs of DOFMS detection.

Focal-Plane Camera. The focal-plane camera (FPC) is a solid-state ion detector comprised of a linear array of discrete charge-collecting Faraday strips. Originally, the FPC was designed to fit along the focal plane of a Mattauch−Herzog mass spectrograph (MHMS).[14,15] Because the MHMS simultaneously disperses ions in space according to m/z, the detector requirements are similar to those of DOFMS. The device incorporated into our DOFMS instrument is the third generation in a series of four detector arrays that have been developed and has 512 Faraday strips, so is referred to as the FPC-512 system.[16−20]

A number of features make the FPC well suited for DOFMS detection. Physically, the FPC employs 512 charge-collecting Faraday strips that are each 8.5 μm wide at a pitch of 12.5 μm; this geometry results in a 6.4 mm-long array with 68% of the array being ion-active. Each Faraday strip has a dedicated integrating amplifier with two levels of gain, controlled by the capacitance in its negative feedback loop; at high gain the FPC has a limit of detection of about 100 charges. Because the FPC is flat and measures the ion flux directly, it provides a direct electrical readout of mass-separated ion-packet widths and the number of ions in each packet. The FPC produces analog signals proportional only to ion charge, eliminating the effect of detector mass bias while providing signal enhancement for multiply charged ions.

The FPC also offers truly simultaneous detection by gating the output signals from all integrating amplifiers into dedicated sample-and-hold amplifiers before serial readout on a shift register. Gating and serial readout are computer-controlled and can be integrated into the DOF timing system. Currently, the FPC has a software-limited data acquisition rate of 10 Hz, making its spectrum-acquisition rate compatible with many chromatographic systems.[21] Experimentally, a dynamic range greater than 10^8 has been reported for the FPC-512, surpassing what is currently available for TOFMS detection.[19] Extended dynamic range detection is especially critical for complex-mixture analysis, where the dynamic range of current methods has been shown to limit the number of detectable compounds.[22] Reported isotope ratio precision better than 0.05% RSD illustrates uniform pixel-to-pixel response across the array.[19] The modern semiconductor fabrication technologies employed to construct the FPC ensure exceptional device-to-device uniformity and a moderate price point for large-scale production. Finally, the FPC-512 has proven to be a very robust detector with over 2 years of operation in two different mass spectrometers with no noticeable decline in performance.

One characteristic in which the FPC-512 falls short is its length. An ideal DOFMS detector would be as long as practical, so the widest range of m/z values could be detected on each ion extraction. The small size of our prototype detector is not a fundamental limitation of solid-state detection technology; a similar detector, 12 cm in length and with 4800 channels, has recently been introduced.[23] For reference, with our current instrument geometry and a 12 cm detection area, almost the entire lanthanide and actinide series could be detected simultaneously, from ^{141}Ce to ^{238}U. A compilation of critical DOFMS detector characteristics with a qualitative comparison between the FPC and the previous generation MCP/phosphor detector is provided in Table 1.

Table 1. Comparison of Modern Detector Arrays with the Ideal DOF Detector[a]

ideal characteristic	FPC[b]	MCP[c]/phosphor
flat, spatially selective detection surface	+	+
simultaneous detection	+	+
long active area	−, [6.4 mm]	0, [25 mm]
dynamic range	+, [10^8]	−, [10^3]
sensitivity (down to single ion strike)	0, [100 charges]	−
no mass bias	+	−
no detector-limited resolution	+	−
uniform signal response along DOF axis	+	−
direct computer control	+	−
fast detection/readout time	0, [50 ms]	−
timing synchronous with DOF separation	+	−
cost	0	+

[a] In this evaluation, a plus/minus (+, 0, −) ranking system indicates the relative ability of the detection system to satisfy ideal needs of DOFMS detection. For some characteristics, the figures of merit are provided in brackets. [b] FPC = focal plane camera. [c] MCP = microchannel plate.

EXPERIMENTAL SECTION

Instrument Description. The DOFMS instrument used in this study has been previously detailed,[3] so only a brief description will be provided here. Our current DOFMS instrument generates singly charged atomic ions with a reduced-pressure, direct-current (dc) glow-discharge (GD) ionization source.[24] After analyte ions are cathodically sputtered from a conductive sample, they are transported to the mass analyzer via a three-stage differentially pumped interface. Upon entrance into the third stage, the ion beam is focused into the CMA extraction region by means of a dc-quadrupole doublet ion optics train.[25,26]

The CMA extraction region consists of two parallel electrodes that are coaxial to the input ion optics. A positive high voltage (HV), square-shaped pulse is applied to the CMA repeller plate, while the gridded, front electrode of the CMA region is held at ground potential. This HV pulse forms a transient electric field that accelerates ions orthogonal to their initial propagation axis.

After CMA extraction, ions traverse a grounded, field-free region according to their spontaneous-drift trajectories[27] until they penetrate the single-stage ion mirror. After emerging from the mirror, ions return to the grounded field-free region before arrival at the DOF extraction region.

The DOF extraction region is comprised of two parallel electrodes that are in line with the mass-separation axis. At a specific detection time (t_{det}) delayed from the onset of the CMA pulse, a +3000 V, 2 μs pulse is applied to the DOF repeller plate in order to generate a constant-energy acceleration (CEA) field that pushes m/z-separated ions upward onto the surface of the FPC. The t_{det} is applied just prior to the energy-focus time to account for transit time of ions from the DOF extraction region to the FPC; t_{det} is adjusted so that ions strike the FPC surface at t_{ef}. CMA and DOF pulse widths, as well as t_{det}, are controlled by a single commercial pulse generator (Berkeley Nucleonics Corporation, San Rafael, CA) operated remotely with LabVIEW (version 8.6, National Instruments, Austin, TX).

FOCAL-PLANE CAMERA INSTALLATION

In order to fit the FPC into our DOFMS instrument, a detector stand was constructed that positions the FPC and its supporting circuit board face down, running along the mass-separation axis

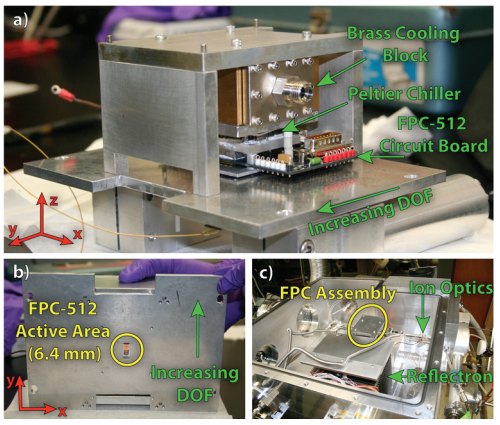

Figure 2. Photographs of FPC installation on DOFMS instrument: (a) The FPC is attached to a mounting apparatus that positions the camera along the DOF field-free region. In this image, mass separation is along the *y*-axis and the DOF extraction pulse pushes ions upward along the *z*-axis. (b) The bottom view of the FPC mounting apparatus shows the FPC active area; the *z*-axis is into the plane of the figure. (c) Inside the DOFMS instrument mass-analysis chamber, the camera is installed at a field-free distance of 281.4 mm.

from flight distances 281.4 to 287.6 mm. Figure 2 documents installation of the FPC-512 into the DOFMS instrument. The face of the camera was positioned at the space-focus plane[5] of the DOF extraction region. To prevent capacitive coupling of the DOF extraction field to camera electronics, a grounded DOF extraction orifice positioned between the DOF extraction region and the FPC face was limited to 1.75 cm × 0.75 cm, with the FPC stationed in the center of this orifice.

Johnson noise was limited by cooling the FPC to −45 °C with a Peltier chiller attached to the back of the circuit board, directly behind the FPC integrated circuit. Heat was removed from the hot side of the Peltier element by a 1:1 mixture of ethylene glycol−water maintained at −18 °C by a recirculating chiller (Neslab Instruments, Inc., Endocal, Newington, NH) and circulated through a brass cooling block fixed directly behind the chiller. UltraTorr Cajon fittings (Swaglok, Solon, OH) were used to feed the cooling liquid into the vacuum chamber.

Electrical connections to the FPC were fed into vacuum by three hermetically sealed μD connectors (Mouser, Mansfield, TX). Power to the FPC and supporting circuit board was supplied by an external supply at 12 V (model 6603D-10, Topward Electric Instruments Co, Taiwan). The Peltier chiller was operated at a current limit of 3.25 A and around 10 V (model 1621A DC, BK Precision, Yorba Linda, CA). The FPC was operated under computer control with LabVIEW through a National Instruments PCI-6281, 18-bit data acquisition card.

Data Acquisition and Processing. The integration time for all pixels on the FPC is software-controlled. Throughout the integration time, the voltage output at each integrating amplifier is simultaneously gated to a dedicated sample-and-hold amplifier (SaHA) and recorded; each readout is termed an "acquisition." If ion flux is constant across the entire integration window, charge accumulates linearly on each pixel and a plot of acquisition voltage vs time is straight. The slope of this plot, along with the gain level of the integrating amplifier indicates the flux of charges impinging on each pixel. Importantly, though slope is most often reported, raw voltages are also obtained for each acquisition within a temporal integration window. Therefore, any changes in

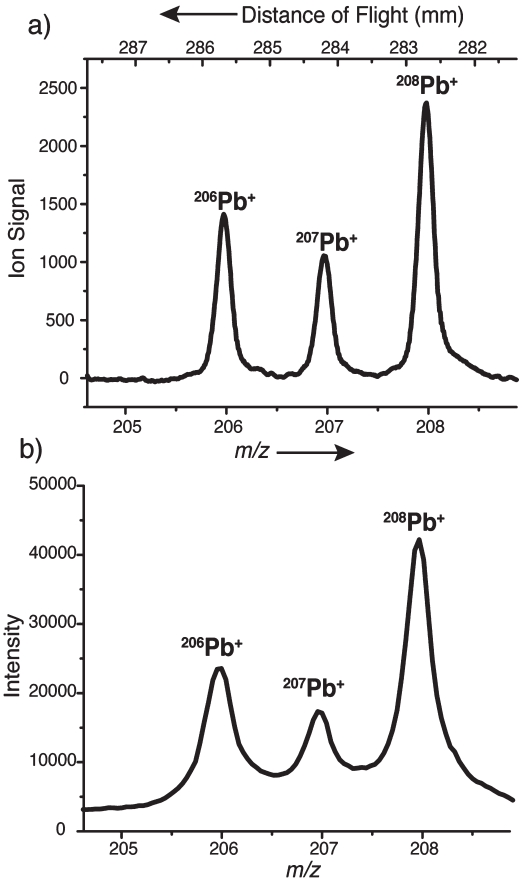

Figure 3. DOFMS mass spectra of lead isotopes obtained with the FPC (a) and MCP/phosphor (b) detectors. Under the instrumental conditions employed here, 4.6 amu can fit along the FPC in the Pb mass range. Improved resolving power and peak shape apparent with the FPC are the result of direct charge detection and minimal image spreading afforded by the FPC.

ion flux within an integration window are identifiable. Consequently, distinct influxes of ions, such as might occur during the elution of a chromatographic peak, can be deconvoluted from a steady background signal. Because the dc-GD is a constant ion source, all ion signals reported here were obtained by the linear-regression method, though various integration periods were used. Following voltage acquisition, the charge on each Faraday strip detection element is neutralized by shorting the capacitance in the negative feed-back loop of the integrating operational amplifier.

All DOF spectra were background-subtracted with a spectrum collected at a t_{det} set to an off-mass region of the DOF spectrum and smoothed (LabVIEW, "Savitzky-Golay Filter.vi"). Resolution for all FPC mass spectra was calculated as $L/\Delta L$ (eq 6), where L is the m/z flight distance and ΔL is the full-width at half-maximum (fwhm) determined from a Gaussian fit to the mass-spectral peak with OriginPro (version 8.5, OriginLab Corporation, North Hampton, MA). Calibration of the DOF spectra to a linear m/z scale was accomplished with a linear fit of $(m/z)^{-1}$ versus DOF.

Sample Preparation. Solid, metallic samples of brass and lead were obtained from the Indiana University Mechanical Instrument Services Department. A metal ingot of tin (National Bureau of Standards, Standard Sample 42d, U.S. Department of Commerce, Washington, DC) was used for tin isotope determination. All samples were analyzed directly with the GD.

dx.doi.org/10.1021/ac201876y |*Anal. Chem.* 2011, 83, 8552–8559

Safety Considerations. This work involved use of high voltages. Care was, and must be, taken with exposed HV on the GD. Otherwise, all exposed potentials were within the mass analyzer and posed no direct health threat.

RESULTS AND DISCUSSION

Mass Resolution with FPC. The first experimental implementation of DOFMS[3] utilized an MCP/phosphor detector assembly and an optical camera to capture images of mass-spectral lines visible on the phosphor plate. This system was cumbersome to operate, required time-consuming image acquisition and off-line processing, and produced convoluted mass spectra due to the various conversion steps in signal amplification and collection.[28] With the MCP/phosphor detection system, peak widths of 0.6−1 mm and mass resolving powers ($R_{(fwhm)}$) of around 400 were obtained across a mass range from 52 − 208 amu.[3] However, it was unclear from these initial studies whether the recorded peak widths were fundamental to the DOF mass-separation technique, dictated by the specific DOFMS design, or a product of the detection system. To overcome the shortcomings of the MCP/phosphor setup, we installed the FPC-512. Since the FPC directly detects charge as ions strike each Faraday strip, the signal from the camera provides a truer representation of DOF peak widths.

Table 2. DOF Mass Resolving Power Attained with FPC

isotope	Δd (fwhm)	$R_{(fwhm)}$
^{40}Ar	300 μm	900
^{63}Cu	250 μm	1100
^{120}Sn	325 μm	860
^{208}Pb	270 μm	1030

Figure 3 compares a DOF mass spectrum of lead isotopes obtained with the FPC to that acquired with our original MCP/phosphor detector. Results with the FPC demonstrate baseline-resolved Pb peaks with linewidths of around 275 μm and $R_{(fwhm)}$ = 1000, whereas the MCP/phosphor produced linewidths of 1000 μm and $R_{(fwhm)}$ = 400. This increase in resolving power is attributable to the improved spatial resolution of the FPC because no other instrumental modifications discriminate the two spectra. Table 2 lists DOFMS linewidths and resolving powers achieved with the FPC for a number of isotopes across the elemental mass range. Differences in resolving power

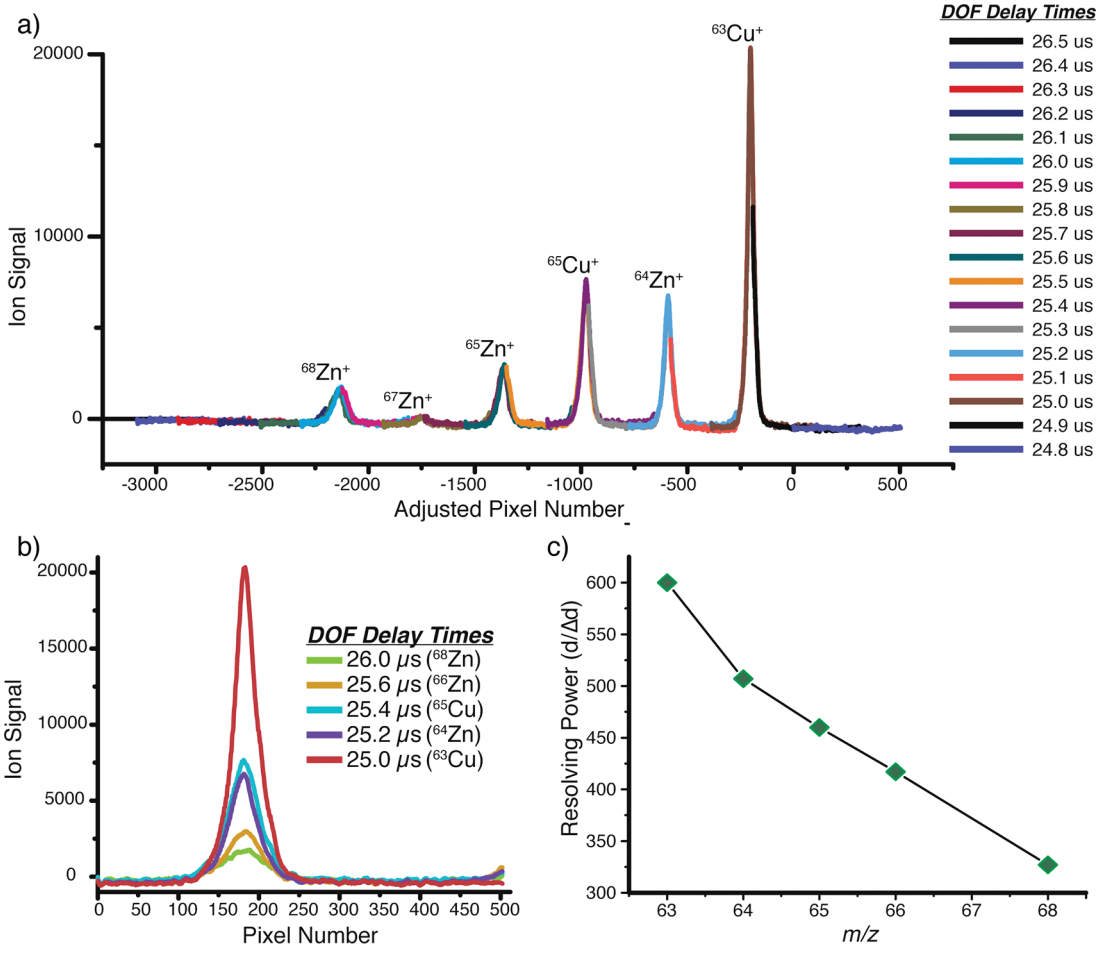

Figure 4. (a) Pixel-shifted spectrum of copper and zinc isotopes shows the representative isotopic distribution. Individual spectra were recorded at 0.1 μs intervals from t_{det} = 24.8−26.5 μs. In order to stitch together a composite spectrum, the average velocity of $^{63}Cu^+$ was determined and each DOF mass spectrum collected at successive DOF delay times was shifted by the number of pixels $^{63}Cu^+$ travels in 0.1 μs. (b) DOF mass spectra collected at five different DOF delay times correspond to five of the Cu and Zn isotopes. Because these mass-separated ion packets strike the FPC at the same position along the array, the resolution achieved cannot be a function of the detector but rather of DOFMS focusing. (c) The best focus is achieved with t_{det} = 25.0 μs. As this delay time changes and other m/z come into the DOF detection window, resolution degrades.

dx.doi.org/10.1021/ac201876y |Anal. Chem. 2011, 83, 8552–8559

between m/z ranges are minimal and are the result of ion-optic focus achieved in any given experiment.

Compared to the MCP/phosphor detection assembly, the FPC yielded peak shapes that are more in keeping with expectations. At linewidths of several hundred micrometers, enough pixels on the FPC are covered to provide reliable peak-shape information. A Gaussian shape is expected because the DOFMS peak should mimic the spatial distribution of ions within the CMA extraction region. A slight tailing toward the high mass, short DOF is also observed and is the result of second-order energy defocusing.[2] All peaks obtained with the FPC fit well to a Gaussian function ($R^2 \geq 0.99$), whereas with the MCP/Phosphor, peaks were less Gaussian-like.

Accessible Mass Range. In DOFMS, ions of all m/z values that exit the reflectron are energy-focused at t_{ef}. However, only ions that are within the DOF detection region at t_{det} and at the field-free lengths covered by the DOF detector after DOF extraction are detectable in a given experiment. The m/z-window observable for a particular detector length (L_D) and the field-free length at the far end of the detector (L_{far}) can be calculated as a ratio of the highest m/z observable $(m/z)_{high}$ to the lowest $(m/z)_{low}$:

$$\frac{(m/z)_{high}}{(m/z)_{low}} = \frac{L_{far}}{L_{near}} = \frac{1}{1 - L_D/L_{far}} \quad (7)$$

With the FPC-512 array positioned at a far field-free distance of 287.8 mm, the high-to-low mass ratio available is 1.023. This ratio corresponds to a mass range of only 4.6 amu when $^{208}Pb^+$ is the high mass of interest, 2.6 amu for $^{120}Sn^+$, and 1.4 amu for $^{64}Zn^+$. In order to expand the detectable mass range with the FPC, two methods have been developed to "scan" a DOF mass spectrum.

The first mass-scanning approach is termed the "pixel-shift" method and is achieved by incrementally changing t_{det} while keeping all other electrostatic potentials constant. As t_{det} is increased, ions with progressively heavier m/z values come into the DOF extraction region at the correct position to strike the FPC. At each selected value of t_{det}, a mass spectrum is recorded. A composite mass spectrum is then assembled by shifting the DOF axis (in pixels) of each component mass spectra by the appropriate distance for each incremental change of t_{det}. The pixel-shifting procedure is straightforward and can be easily automated in order to "scan" a broader m/z range with a single DOF detector of limited length. Figure 4a is a composite spectrum of the copper and zinc isotopes acquired with 17 different DOF delay times and assembled with the pixel-shift method. Figure 4a clearly indicates the isotopic distribution of copper and zinc and is displayed with the DOF axis running left to right; the conventional m/z axis would run right to left.

Unfortunately, this pixel-shifted approach comes at a price: with constant CMA and reflectron conditions, true energy focus is achieved for only a single DOF spectrum within the pixel-shifted composite and resolution degrades as t_{det} moves away from the energy-focused detection time. This point is illustrated in Figure 4, in which focus was optimized for $^{63}Cu^+$ at $t_{det} = 25.0\ \mu s$. Figure 4b gives overlaid, nonpixel-shifted DOF mass spectra of the copper and zinc isotopes. In Figure 4c, a plot of the resolving power of these spectra versus m/z demonstrates a decline in resolving power as t_{det} moves away from 25.0 μs.

Though the pixel-shift method causes resolution to degrade with t_{det}, loss of resolving power with m/z is not intrinsic to

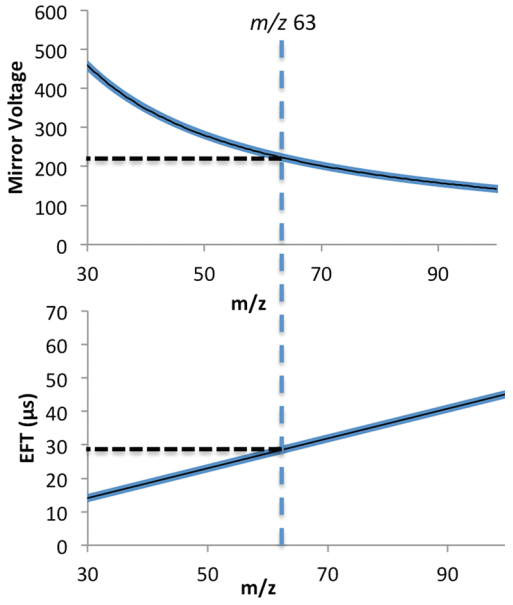

Figure 5. With constant-momentum acceleration (CMA), the ion-mirror voltage (V_M) can be changed to bring ions of any m/z value of interest to the DOF detection distance (L) at the energy-focus time (t_{ef}). The plots above relate V_M and t_{ef} to m/z for a CMA pulse of +400 V and 0.75 μs. The intersection of a vertical line across the stacked plots gives the appropriate V_M and t_{ef} for a particular m/z.

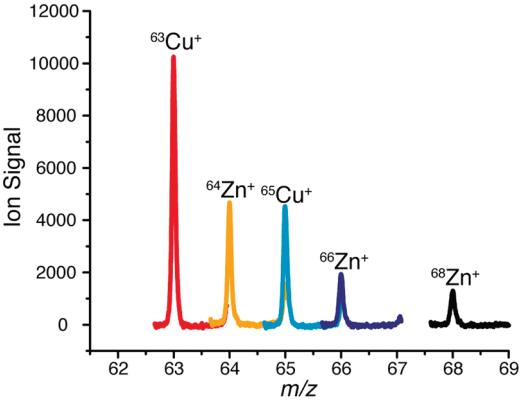

Figure 6. Five independent, energy-focused mass spectra of the copper and zinc isotopes are shown in this composite mass spectrum. Consistent resolution across all m/z is achieved with the energy-focused mass-range switching approach.

DOFMS. In fact, optimal resolving power along the DOF axis is available for ions of all m/z values at t_{ef}.

In order to take advantage of the focusing ability of DOFMS, a second mass-scan method was developed in which a stitched spectrum is generated by sequentially bringing ions of various m/z values onto the detector at their proper energy-focus times. As shown in eqs 4 and 5, the t_{ef} and L of a particular m/z is a function only of electrostatic potentials. In particular, if CMA conditions are held constant, changing the ion-mirror potential (V_M) and the DOF delay time (t_{det}) at a set ratio permits DOF detection of many different m/z ranges at several unique, m/z-specific energy-focus times. Figure 5 illustrates how the mirror voltage and detection time were chosen to bring ions of a particular m/z onto the FPC. In order to assemble a complete mass spectrum,

dx.doi.org/10.1021/ac201876y |Anal. Chem. 2011, 83, 8552–8559

Table 3. Instrumental Conditions and Results for Energy-Focused Mass-Range Switching

m/z (Th)	mirror voltage (V)	DOF delay time (μs)	DOF line width (fwhm) (μm)	resolving power ($d/\Delta d$)
63	227.5 (228.3)[a]	27.92 (27.85)[a]	378	750
64	225.9 (224.9)[a]	28.47 (28.27)[a]	363	790
65	222.3 (221.6)[a]	28.89 (28.70)[a]	390	730
66	218.9 (218.1)[a]	29.13 (29.15)[a]	402	710
68	212.8 (212)[a]	30.03 (30.00)[a]	390	700

[a] Values listed in parentheses were calculated from fundamental principles to bring each m/z of interest onto the DOF detector at a flight distance of 286 mm.

each DOF spectrum was independently mass-calibrated and then compiled on a single m/z axis. Figure 6 provides a stitched mass spectrum of the copper and zinc isotopes obtained in five independent mass windows. Table 3 lists the experimental conditions with calculated values shown parenthetically and the resolving power obtained with this energy-focused mass-scan method. Table 3 verifies that DOFMS is performing as predicted by theory. Resolution does not significantly degrade between mass windows, which indicates that all m/z are energy-focused. Also, the mirror values and detect times that were calculated from theory almost exactly match experimental results without adding any instrumental correction factors.

Implementation of the energy-focused mass-scan method illustrates that a small, stationary DOF detector can be used to rapidly switch between mass ranges. Because this mass-range switching requires simply changing electrostatic potentials, detector response and readout times control how quickly different mass windows can be acquired. With the FPC-512, mass ranges can be switched every 100 ms if ion flux is high enough and substitution of a larger DOF detector will enhance the efficiency of this technique because larger m/z windows can be acquired at each t_{det}.

The development of both the pixel-shift and energy-focused mass-scan methods for DOFMS analysis demonstrates that any m/z of interest can be measured with a stationary DOF detector by simple electrostatic changes. These m/z ranges can be analyzed sequentially as reported here or in any more complicated sequence required by a particular experiment, such as dictated by analyte elution times from a chromatographic run. With DOFMS employed to analyze a specific m/z range, detection improvements such as enhanced linear dynamic range and charge-based detection that are intrinsic to the FPC can be realized. The on-demand separation of the m/z of interest in space also opens possibilities for m/z-specific isolation and collection. Finally, the small m/z-window currently available for simultaneous detection is not a fundamental weakness of DOFMS but rather a limitation imposed by the active detection length of the FPC-512.

CONCLUSIONS

Incorporation of the FPC into the DOFMS platform is a major step toward realizing the potential of DOFMS. Initial results with this array detector show improved mass resolution and the use of two simple mass-scan methods to expand the mass range available for DOF detection. Upcoming investigations will provide analytical figures of merit for the FPC-DOFMS combination. In addition, there are several aspects of DOFMS that require more work. Foremost is the ability of DOFMS to achieve simultaneous m/z separation across a wide mass range. In order to achieve this goal, a new DOFMS detection setup will be constructed that will allow the FPC to be positioned at different places along the DOF axis. Additionally, an automated computer-control system is being designed that will sequentially bring widely different mass ranges into optimal focus at a single, stationary FPC. In particular, a "peak-hopping" protocol will allow several m/z ranges of interest to be determined within the time frame of a chromatographic peak. This peak-hopping method might be particularly useful for complex-mixture analysis, where the benefits of the extended dynamic range FPC will be experimentally examined. Also, a longer 1696-channel FPC is currently being characterized with a MHMS in our lab and will be employed with DOFMS. Several recent reports of novel, spatially selective array detectors underline an expanding level of interest in dispersive MS detection; these detectors could provide alternative avenues for DOFMS growth.[7,29,30]

AUTHOR INFORMATION

Corresponding Author
*E-mail: Hieftje@indiana.edu.

ACKNOWLEDGMENT

The authors would like to thank the Indiana University Edward G. Bair Mechanical Instrumentation Facility as well as IU Electronic and Mechanical Services. This work was supported in part by the U.S. Department of Energy through Federal Grant Number DE-FG02-98EF14890, by the Lilly Endowment-Indiana MetaCyt Initiative, and by Laboratory Directed Research & Development (LDRD) funds from Pacific Northwest National Laboratory (operated by Battelle Memorial Institute under contract to the U.S. Department of Energy).

REFERENCES

(1) Enke, C. G. The Unique Capabilities of Time-of-Flight Mass Analyzers. In *Advances in Mass Spectrometry*; Elsevier Science Publishers B. V.: Amsterdam, The Netherlands, 1998; Vol. 14, pp 197−219.
(2) Enke, C. G.; Dobson, G. S. *Anal. Chem.* **2007**, *79* (22), 8650–8661.
(3) Graham, A.; Ray, S.; Enke, C.; Barinaga, C.; Koppenaal, D.; Hieftje, G. *J. Am. Soc. Mass Spectrom.* **2011**, *22* (1), 110–117.
(4) Wolff, M. M.; Stephens, W. E. *Rev. Sci. Instrum.* **1953**, *24* (8), 616–617.
(5) Cotter, R. J. *Time-of-Flight Mass Spectrometry*; American Chemical Society: Washington, DC, 1994; Vol. 549.
(6) Barnes, J. H.; Hieftje, G. M. *Int. J. Mass Spectrom.* **2004**, *238* (1), 33–46.
(7) Koppenaal, D. W.; Barinaga, C. J.; Denton, M. B.; Sperline, R. P.; Hieftje, G. M.; Schilling, G. D.; Andrade, F. J.; Barnes, J. H., IV *Anal. Chem.* **2005**, *77* (21), 418 A–427 A.
(8) Hannay, N. B.; Ahearn, A. J. *Anal. Chem.* **1954**, *26* (6), 1056–1058.
(9) Beynon, J. H.; Jones, D. O.; Cooks, R. G. *Anal. Chem.* **1975**, *47* (11), 1734–1738.
(10) Giffin, C. E.; Boettger, H. G.; Norris, D. D. *Int. J. Mass Spectrom. Ion Phys.* **1974**, *15* (4), 437–449.

(11) Aberth, W. *Int. J. Mass Spectrom. Ion Phys.* **1981**, *37* (3), 379–382.
(12) Froesch, M.; Luxembourg, S. L.; Verheijde, D.; Heeren, R. M. A. *Eur. J. Mass Spectrom.* **2010**, *16* (1), 35–45.
(13) Birkinshaw, K. *J. Mass Spectrom.* **1997**, *32* (8), 795–806.
(14) Burgoyne, T. W.; Hieftje, G. M.; Hites, R. A. *J. Am. Soc. Mass Spectrom.* **1997**, *8* (4), 307–318.
(15) Knight, A. K.; Sperline, R. P.; Hieftje, G. M.; Young, E.; Barinaga, C. J.; Koppenaal, D. W.; Denton, M. B. *Int. J. Mass Spectrom.* **2002**, *215* (1−3), 131–139.
(16) Barnes; Sperline, R.; Denton, M. B.; Barinaga, C. J.; Koppenaal, D.; Young, E. T.; Hieftje, G. M. *Anal. Chem.* **2002**, *74* (20), 5327–5332.
(17) Barnes; Schilling, G. D.; Sperline, R.; Denton, M. B.; Young, E. T.; Barinaga, C. J.; Koppenaal, D. W.; Hieftje, G. M. *Anal. Chem.* **2004**, *76* (9), 2531–2536.
(18) Schilling, G. D.; Andrade, F. J.; Barnes; Sperline, R. P.; Denton, M. B.; Barinaga, C. J.; Koppenaal, D. W.; Hieftje, G. M. *Anal. Chem.* **2006**, *78* (13), 4319–4325.
(19) Schilling, G. D.; Ray, S. J.; Rubinshtein, A. A.; Felton, J. A.; Sperline, R. P.; Denton, M. B.; Barinaga, C. J.; Koppenaal, D. W.; Hieftje, G. M. *Anal. Chem.* **2009**, *81* (13), 5467–5473.
(20) Felton, J. A.; Schilling, G. D.; Ray, S. J.; Sperline, R. P.; Denton, M. B.; Barinaga, C. J.; Koppenaal, D. W.; Hieftje, G. M., *J. Anal. At. Spectrom.* **2011**, *26* (2), 300−304.
(21) Barnes, J. H.; Schilling, G. D.; Sperline, R. P.; Denton, M. B.; Young, E. T.; Barinaga, C. J.; Koppenaal, D. W.; Hieftje, G. M. *J. Anal. At. Spectrom.* **2004**, *19* (6), 751–756.
(22) Enke, C. G.; Nagels, L. J. *Anal. Chem.* **2011**, *83* (7), 2539–2546.
(23) SPECTRO MS Fully Simultaneous ICP-Mass Spectrometer. Ametek Materials Analysis Division, 2011.
(24) McClenathan, D. M.; Hieftje, G. M. *J. Anal. At. Spectrom.* **2005**, *20* (12), 1326–1331.
(25) Rogers, D. A.; Ray, S. J.; Hieftje, G. M. *Metallomics* **2009**, *1* (1), 67–77.
(26) Myers, D. P.; Li, G.; Mahoney, P. P.; Hieftje, G. M. *J. Am. Soc. Mass Spectrom.* **1995**, *6* (5), 400–410.
(27) Guilhaus, M. *J. Am. Soc. Mass Spectrom.* **1994**, *5* (6), 588–595.
(28) Edgar, M. L.; Kessel, R.; Lapington, J. S.; Walton, D. M. *Rev. Sci. Instrum.* **1989**, *60* (12), 3673–3680.
(29) Hadjar, O.; Johnson, G.; Laskin, J.; Kibelka, G.; Shill, S.; Kuhn, K.; Cameron, C.; Kassan, S. *J. Am. Soc. Mass Spectrom.* **2011**, *22* (4), 612–623.
(30) Bamberger, C.; Renz, U.; Bamberger, A. *J. Am. Soc. Mass Spectrom.* **2011**, *22* (6), 1079–1087.